IEEE Photonics Journal
An IEEE Photonics Society Publication

Open Access

Measurement of the Dispersion of an Antiresonant Hollow Core Fiber

Volume 10, Number 4, August 2018

Teodora Grigorova
Rudrakant Sollapur
Andreas Hoffmann
Alexander Hartung
Anka Schwuchow
Jörg Bierlich
Jens Kobelke
Markus A. Schmidt
Christian Spielmann

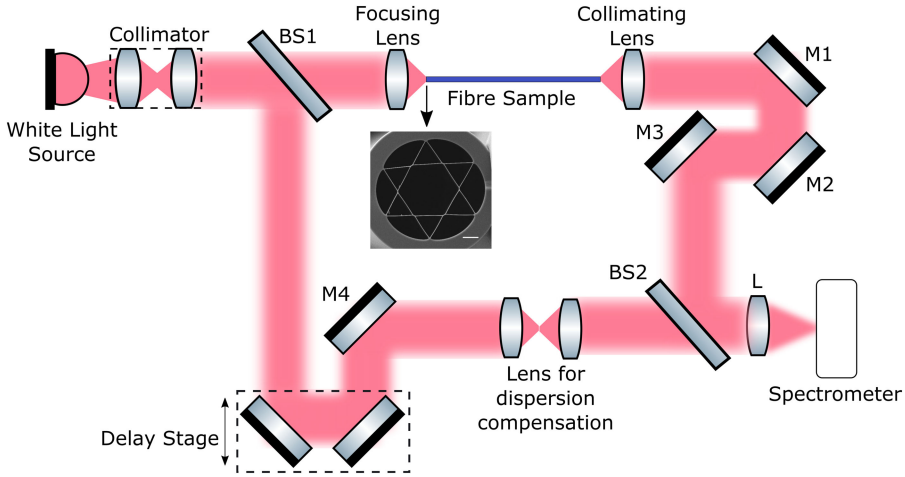

DOI: 10.1109/JPHOT.2018.2861226
1943-0655 © 2018 IEEE

IEEE photonics SOCIETY

IEEE

Measurement of the Dispersion of an Antiresonant Hollow Core Fiber

Teodora Grigorova,[1] Rudrakant Sollapur,[1] Andreas Hoffmann,[1] Alexander Hartung,[2] Anka Schwuchow,[2] Jörg Bierlich,[2] Jens Kobelke,[2] Markus A. Schmidt,[2,3] and Christian Spielmann[1,4]

[1]Institute of Optics and Quantum Electronics, Abbe Center of Photonics, Friedrich Schiller University, Jena 07743, Germany
[2]Leibniz Institute of Photonic Technology e.V., Jena 07745, Germany
[3]Otto Schott Institute of Material Research, Abbe Center of Photonics, Friedrich Schiller University, Jena 07743, Germany
[4]Helmholtz Institute Jena, Jena 07743, Germany

DOI:10.1109/JPHOT.2018.2861226

Manuscript received July 5, 2018; accepted July 25, 2018. Date of publication July 31, 2018; date of current version August 14, 2018. This work was supported by the German Research Foundation via the International Research Training Group 2101, Federal state of Thuringia (FKZ: 2012FGR0013, FKZ 2016FGR0051), and European Science Foundation (ESF) under Project no. 2016FGR0051. Corresponding author: C. Spielmann (e-mail: Christian.spielmann@uni-jena.de).

Abstract: Due to unique properties, antiresonant hollow core fibers have found widespread use in various fields of science and application. Particular regarding applications that involve ultrashort pulses, precise knowledge of group velocity dispersion is essential to understand the underlying physics and to optimize device performance. Here we report on the successful measurement of the spectral distribution of the group velocity dispersion of the fundamental mode of an antiresonant hollow core fiber in close proximity to and away from a strong strand resonance. The results show the variations of the hundreds of fs^2/cm near the resonance region, whereas the dispersion is identical to that of a perfect cylindrical waveguide away from the resonance in accordance with a literature. An additional zero dispersion wavelength that is not present in the case of a capillary was experimentally verified. The possibility to tune dispersion via strand resonances opens up a novel pathway towards engineering pulse dispersion, with applications in fields such as nonlinear science and pulse propagation management.

Index Terms: Antiresonant hollow core fiber, dispersion measurement.

1. Introduction

Antiresonant hollow core fibers (ARHCFs) [1], [2] are attracting great attention in recent times due to low propagation losses over large spectral bandwidth, large core dimensions and a comparable simple fabrication scheme. Depending on the microstructure used, the antiresonant effect leads to a discrete number of transmission bands limited by regions of high loss, which are associated with geometry-induced (i.e., strand) resonances that allow to light the transversely transmit through the microstructure [2], [3]. Due to their unique properties ARHCFs have been identified as future platforms for nonlinear optics [4], [5], sensing [6], high power delivery [7] and telecommunication [8]. Various types of ARHCF geometries such as the negative curvature [3], [9], the double revolver [10], the single ring [11] or the hypocycloid core contour [12] designs have been recently implemented,

showing low optical losses at mid and near infrared [3], [5], [13], visible and even at UV wavelengths [2], [5].

Nonlinear light generation, in particular supercontinuum generation and ultrashort pulse transportation demand precise knowledge on modal pulse dispersion of the waveguide used to optimize device performance [14]. As shown for instance in [15] group velocity dispersion (GVD) in ARHCFs is generally low (few fs^2/cm) being close to that of a cylindrical waveguide with perfectly reflecting walls and is dominated by the material inside the core section of the fiber [16]. In the vicinity of strand resonances, however, dispersion is strongly modified and can change by orders of magnitude. This dispersion modification has been utilized in a recent study to generate three-octave spanning supercontinua down to UV wavelengths in a krypton filled ARHCF [4]. Since the resonance-induced contribution dominates the GVD close to the resonances, this type of dispersion management scheme uniquely allows for power scaling by increasing core diameters while maintaining the dispersion properties. All these points clearly emphasize that precise experimental data on the spectral distribution of the GVD is highly important, in particular from the standpoint that the properties of the propagating modes get substantially more complex when spectrally approaching the resonance.

In this work, we measure the spectral dependence of the GVD of an ARHCF over a considerable bandwidth on both sides of a strand resonance. By using an interferometric technique, we determine the accumulated phase of a femtosecond pulse propagating through a single ring ARHCF and apply an established data analysis procedure [17] to obtain the distribution of the GVD at visible and near infrared wavelengths.

2. Antiresonant Hollow Core Fiber (ARHCF)

The operational principle of ARHCFs relies on the fundamental mode not being phase-matched (i.e., antiresonant) to any other mode in the system [1] – a situation requiring a sophisticated microstructured cladding with a low number of well-engineered modes or resonances to reduce losses to acceptable levels. In a typical gas- or air-filled ARHCF geometry, resonances are obtained at those wavelengths, where the light can transmit through the glass strand surrounding the core, yielding high loss at characteristic wavelengths given by $\lambda = 2t\sqrt{n^2 - 1}/m$ (t: thickness, m: mode order; n: refractive index of silica). These high losses strongly impact the spectral evolution of the phase index, which forms the underlying reason for the GVD modification in spectral vicinity of a strand resonance.

The ARHCF used here consists of a large hollow core (diameter $\approx$ 50 μm) surrounded by a single-ring silica microstructured cladding (inset in Fig. 1(a)) with an average strand thickness of $\sim$450 nm. Due to the nanometer thickness of the strands, this fiber design supports a fundamental core mode within three transmission bands located at visible and near-IR wavelengths (Fig. 1).

3. Method and Measurements

Here the dispersion of the ARHCF shown in Fig. 1 was measured through spectral interferometry [17]. This method ensures accurate determination of the GVD of the fiber in case of a perfectly balanced interferometer and is very robust against experimental errors (e.g., vibrations or source intensity fluctuations). Theoretical considerations predict that ARHCFs have very low GVD of few fs^2/cm within the low-loss transmission bands over hundreds of nanometers and large GVD up to ps^2/cm close to the resonances [18]. So, a fiber length of 9.7 cm was chosen here to observe the interference pattern on the spectrometer with a given resolution. The chosen length not only ensured the measurement of the low GVD region in the broad transmission range, but also recording the finely spaced fringes close to the resonances enabling the determination of the strongly varying GVD.

In the experiment the ARHCF was placed in the sample arm of a compensated Mach-Zehnder interferometer, illuminated by a white-light fiber supercontinuum source (Fianium), as shown in Fig. 2(a). An additional bandpass filter for the visible (FGS900, Thorlabs) inserted before the interferometer attenuated the pump peak of the supercontinuum source. Light was coupled into and out of the ARHCF by two identical lenses (focal length 30 mm). To balance the dispersion in

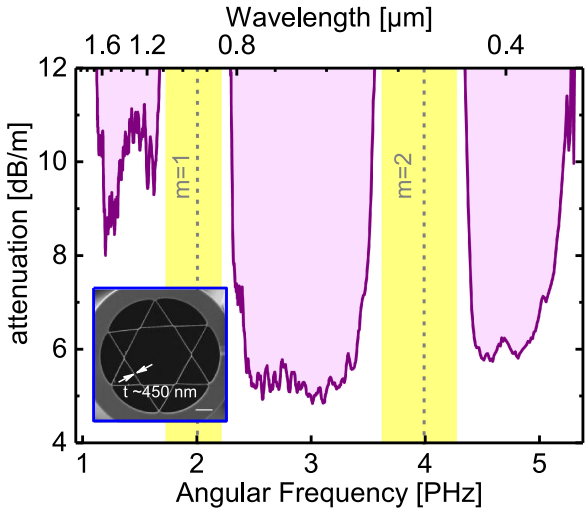

Fig. 1. Measured spectral distribution of the modal attenuation of the fundamental core mode of the antiresonant hollow core fiber. A scanning electron micrograph is shown in the inset. The white horizontal scale bar indicates a length of 10 μm.

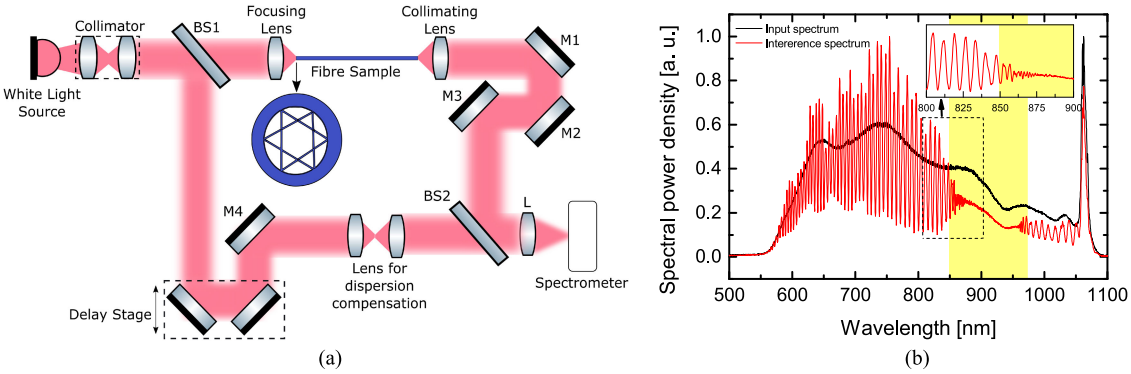

Fig. 2. Setup and measurement: (a) Experimental setup for the measurement of fiber dispersion by spectral interference method, comprising a balanced Mach-Zehnder interferometer with a delay stage in the reference arm and fiber sample in the measurement arm. (b) recorded spectrum with spectral interference in red [inset: spectral interference close to resonance].

the interferometer we included the same lens pair also into the reference arm. Two identical thin glass plates were used as beam splitters, so that ≈96% of the power was guided through the ARHCF and ≈4% through the reference arm. At the output of the interferometer the two beams were combined, and their interference in the spectral domain were observed with a high-resolution spectrometer (HR4000, OceanOptics) as shown in Fig. 2(b). The inset shows the spectral fringe pattern recorded closer to the resonance wavelength, whereas the high loss at the resonance wavelength prevents us from determining the GVD. The interferometric fringes contain information on the dispersion of the ARHCF as function of wavelength. The phase was extracted from the recorded spectrograms using the Fourier-transform method as discussed in [16]. The method was chosen for data analysis due to its reduced sensitivity to the amplitude of the spectrograms, meaning that the losses from absorption and scattering in the interferometer arms do not affect the phase acquisition and phase information can be extracted at all frequencies where fringes are recorded. The recorded spectrogram $S(\omega)$ can be described by $S(\omega) = S_r(\omega) + S_s(\omega) + 2\sqrt{S_r(\omega)S_s(\omega)}\cos(\omega)$ ($S_r(\omega)$ and $S_r(\omega)$: power spectral densities of reference and signal arm, respectively; $\varphi(\omega)$: phase difference between the optical fields propagated through the reference and sample arm).

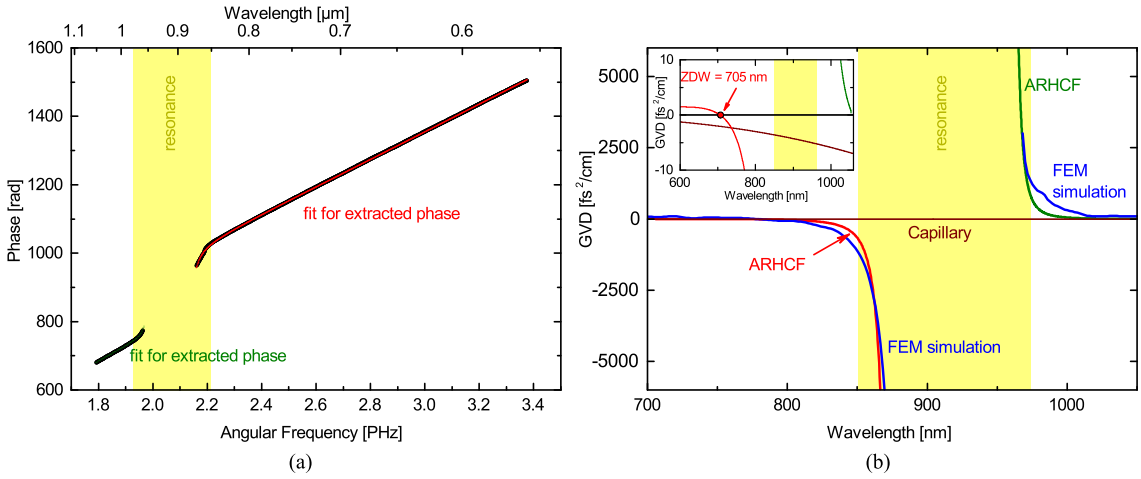

Fig. 3. Calculation of fiber dispersion (a) phase extracted (black line) from the recorded spectrum and fitted with Lorentzian-like resonances (red and green lines) (b) GVD calculated from the fit to the measured phase profile (red and green lines) in comparison with GVD of a standard capillary (in brown) having similar core size calculated by Marcatili-Schmeltzer (MS) model [16] and GVD calculated from FEM simulations for the same fiber using COMSOL (blue) [inset: close-up showing the abrupt GVD variation close to the fundamental strand resonance. Indicated is also the ZDW at 705 nm which in not present in the case of a capillary waveguide].

The spectral distribution of the GVD of the ARHCF was determined from extracting the phase ($\varphi(\omega)$) and its variation with wavelength from the recorded spectrogram. Fig. 3(a) shows the extracted phase (black thick line) from the interference pattern and the corresponding mathematical fits on both sides of the resonance (red and green lines). It is important to note that the density of the interference fringes suddenly increases near resonance. Hence, it is challenging to represent both low and high frequency variations using Taylor expansion for extracted phase information.

Here we assume that the strands surrounding the core behave like high-finesse Fabry-Pérot etalons under oblique incidence. This assumption is justified by the fact that for a tube-type single ring ARHCF with a core diameter that is much larger than the operation wavelength, the modal properties of the propagating mode can be calculated by assuming a wave that is reflected at a corresponding planar film [15]. Considering that we assume here that the phase evolutions can be approximated by Lorentzian-type line shape functions, which are comparable to typical Sellmeier equations used to fit material refractive index data. Equation 1 shows the fitting function used for the phase extracted via spectral interferometry:

$$\varphi = P\omega\sqrt{1 - \frac{A}{\omega^2} - \frac{B\,(\omega - C)}{(\omega - C)^2 + D}} \tag{1}$$

where the first two terms under square root correspond to capillary dispersion, and the third term models the respective resonance with fitting parameters P, A, B, C and D. The parameters P, A and the parameters B, C, D were separately fitted in the spectral ranges of low (i.e., capillary-type) and high dispersion, respectively. Here, one additional resonance term is sufficient to fit well the extracted phase. The addition of more resonance terms to Eq. 1 reduces the error of the fit, but the obtained frequencies usually do not correspond to the expected resonance frequency of the fiber and thus lead to additional and unphysical modulations when calculating the GVD.

Special care was taken to characterize the dispersion in the spectral range from 570 to 860 nm between the two strand resonances of lowest order (m = 1 and m = 2) because its crucial for supercontinuum generation using pump pulses from Ti:sapphire laser systems at 800 nm [4]. The phase was extracted (black dots in Fig. 3(a)) from 10 spectrograms recorded at the same delay in the reference arm, and fitted on both sides of the resonance using Eq. 1 (colored curves

TABLE 1
Fitting Parameters for Extracted Phase

Parameter	Below resonance wavelength		Above resonance wavelength	
	Value	Standard deviation	Value	Standard deviation
P	437.40748	6.03683	416.11277	5.83027
A	-1.69159	0.28612	0.51128	0.07684
B	0.00843	7.24836E-4	3.7306E-4	1.16701E-4
C	2.00917	0.02758	1.969	0.00113
D	-0.03697	0.06828	7.83588E-6	4.59314E-6

in Fig. 3(a)). Fig. 3(b) shows the GVD profile of the ARHCF obtained from the fit. The results indicate low and capillary-like dispersion away from the resonance which is strongly modified on both sides of the resonance with an additional zero dispersion wavelength at 705 nm (as shown in the inset), which is not present in case of a capillary (brown curve in Fig. 3(b)). The origin of the group velocity dispersion variation can be qualitatively understood when inspecting Eq. 25 of Ref. [15]: Here the capillary-like distribution of the real part of the effective mode index (term that is proportional to $1/R^2$) is modified by resonance term (term that is proportional to $1/R^3$) that includes the properties of the resonance, i.e., a phase that depends on the refractive indices involved, the strand thickness and the operation wavelength. The particular quantity clearly reveals that from the structural perspective the spectral position of the resonance is dominated by the strand width, suggesting a straightforward dispersion tuning scheme via engineering the microstructure of the fiber, which is impossible to achieve in unstructured capillary waveguides. The difference in radius dependence of the two mentioned terms of Eq. 25 of Ref. [15] additionally shows that structural-resonance imposed dispersion tuning is more strong in fibers which smaller cores, which has obvious implications on waveguide design particular with regard to nonlinear light generation and pulse compression. The spectral distribution of the GVD calculated from finite element method (FEM) simulations (COMSOL) [19] is also shown in Fig. 3(b) (blue curve). These calculations are based on a fixed strand thickness of 450 nm and thus yield a narrow resonance region, whereas the ARHCF used in the experiment has about 10% variation in strand thickness along the length of the fiber and across the cross section of the core at a constant longitudinal coordinate. This variation leads to a broadening of the resonance region to hundreds of nanometer. To match experimental data, the GVD calculated using FEM has spectrally been shifted, showing significant overlap with measured data and thus confirming the large variation in GVD on both sides of the resonance region.

Due to high modal attenuation at the resonance wavelength, the dispersion profile is discontinuous, whereas that spectral region is not relevant for application due to exceedingly high loss. Additionally, we want to mention that the evolution of the GVD is different on both sides of the resonance requiring separate fitting for both ranges (corresponding fit parameters that may serve as starting values for future studies involving fitting are tabulated in Table 1).

The comparable large spectral bandwidth of the discontinuous GVD region is a result of inevitable strand thickness variation along the fiber and across its cross section, which directly impact the resonance. It is important to note that the variation of GVD that is induced by the strand resonance is, to a first-order approximation, independent of core geometry and mostly depends on the thickness of the inner dielectric annulus. This makes it possible to design large core ARHCF with customized and engineered GVD profiles that are beyond what is achievable with typically used fibers, thus enabling to scale high powers within nonlinear light generation schemes. It is indeed possible to control the resonance position and hence the GVD profile of the ARHCF by carefully choosing the strand thickness. Having successfully measured the evolution of GVD near the resonance region,

we observed strong variation of the GVD profile in ARHCF in agreement with simulations [15]. By minimizing the strand thickness variation during fiber drawing, it will be possible to reduce the bandwidth of the resonance thus reducing the discontinuity region of the GVD.

4. Conclusion

In conclusion, we report on successful measurement of the spectral distribution of the GVD of fundamental mode in ARHCF in proximity and away from a geometry-induced resonance showing variations of hundreds of fs^2/cm near the resonance region, whereas otherwise dispersion is low. An additional zero dispersion wavelength, which is not present in the case of capillary-type waveguide was experimentally verified. By controlling the strand thickness the position of resonance wavelength can be precisely tuned paving way for designing fibers with unique dispersion properties with applications in supercontinuum generation, telecommunication and beam delivery.

References

[1] N. Litchinitser, A. Abeeluck, C. Headley, and B. Eggleton, "Antiresonant reflecting photonic crystal optical waveguides," *Opt. Lett.*, vol. 18, pp. 1592–1594, 2002.

[2] A. Hartung *et al.*, "Low-loss single-mode guidance in large-core antiresonant hollow-core fibers," *Opt. Lett.*, vol. 14, pp. 3432–3435, 2015.

[3] A. D. Pryamikov, A. S. Biriukov, A. F. Kosolapov, V. G. Plotnichenko, S. L. Semjonov, and E. M. Dianov, "Demonstration of a waveguide regime for a silica hollow-core microstructured optical fiber with a negative curvature of the core boundary in the spectral region >3.5 μm," *Opt. Exp.*, vol. 19, pp. 1441–1448, 2011.

[4] R. Sollapur *et al.*, "Resonance-enhanced multi-octave supercontinuum generation in antiresonant hollow-core fibers," *Light Sci. Appl.*, vol. 6, 2017, Art. no. e17124. doi: 10.1038/lsa.2017.124.

[5] M. Cassataro *et al.*, "Generation of broadband mid-IR and UV light in gas-filled single-ring hollow-core PCF," *Opt. Exp.*, vol. 25, pp. 7637–7644, 2017.

[6] R. Gao, Y. Jiang, and Y. Zhao, "Magnetic field sensor based on anti-resonant reflecting guidance in the magnetic gel-coated hollow core fiber," *Opt. Lett*, vol. 39, pp. 6293–6296, 2014.

[7] M. Michieletto, J. K. Lyngsø, C. Jakobsen, J. Lægsgaard, O. Bang, and T. T. Alkeskjold, "Hollow-core fibers for high power pulse delivery," *Opt. Exp.*, vol. 24, pp. 7103–7119, 2016.

[8] J. R. Hayes *et al.*, "Antiresonant hollow core fiber with an octave spanning bandwidth for short haul data communications," *J. Lightw. Technol.*, vol. 35, no. 3, pp. 437–442, Feb. 2017.

[9] F. Yu and J. Knight, "Negative curvature hollow-core optical fiber," *IEEE J. Sel. Topics Quantum Electron*, vol. 2, no. 2, Mar./Apr. 2016, Art. no. 4400610.

[10] A. F. Kosolapov *et al.*, "Hollow-core revolver fibre with a double-capillary reflective cladding," *Quantum Electron.*, vol. 46, no. 3, pp. 267–270, 2016.

[11] N. Edavalath, M. H. Frosz, J. Ménard, and P. St. J. Russell, "Fabrication and side-coupling characterization of hexagonal lattice single-ring hollow-core PCFs," in *Proc. Int. Conf. Frontiers Opt.*, 2015, Paper FM3G.3.

[12] F. Yu, W. J. Wadsworth, and J. C. Knight, "Low loss silica hollow core fibers for 3–4 μm spectral region," *Opt. Exp.*, vol. 20, pp. 11153–11158, 2012.

[13] B. Debord *et al.*, "Ultralow transmission loss in inhibited-coupling guiding hollow fibers," *Optica*, vol. 4, pp. 209–217, 2017.

[14] M. Nisoli *et al.*, "Compression of high-energy laser pulses below 5 fs," *Opt. Lett.*, vol. 8, pp. 522–524, 1997.

[15] M. Zeisberger and M. A. Schmidt, "Analytic model for the complex effective index of the leaky modes of tube-type anti-resonant hollow core fibers," *Sci. Rep.*, vol. 7, 2017, Art. no. 11761.

[16] E. A. J. Marcatili and R. A. Schmeltzer, "Hollow metallic and dielectric waveguides for long distance optical transmission and lasers," *Bell Syst. Tech. J.*, vol. 43, no. 4, pp. 1783–1809, Jul. 1964, doi: 10.1002/j.1538-7305.1964.tb04108.x.

[17] T. Grósz, A. Kovács, M. Kiss, and R. Szipőcs, "Measurement of higher order chromatic dispersion in a photonic bandgap fiber: Comparative study of spectral interferometric methods," *Appl. Opt.*, vol. 53, no. 9, pp. 1929–1937, 2014.

[18] M. Zeisberger, A. Tuniz, and M. A. Schmidt, "Analytic model for the complex effective index dispersion of metamaterial-cladding large-area hollow core fibers," *Opt. Exp.*, vol. 24, pp. 20515–20528, 2016.

[19] COMSOL Multiphysics, COMSOL AB, Stockholm, Sweden. [Online]. Available: www.comsol.com.